

Stereotyped connectivity and computations in higher-order olfactory neurons

Mehmet Fişek & Rachel I Wilson

In the first brain relay of the olfactory system, odors are encoded by combinations of glomeruli, but it is not known how glomerular signals are ultimately integrated. In *Drosophila melanogaster*, the majority of glomerular projections target the lateral horn. Here we show that lateral horn neurons (LHNs) receive input from sparse and stereotyped combinations of glomeruli that are coactivated by odors, and certain combinations of glomeruli are over-represented. One morphological LHN type is broadly tuned and sums input from multiple glomeruli. These neurons have a broader dynamic range than their individual glomerular inputs do. By contrast, a second morphological type is narrowly tuned and receives prominent odor-selective inhibition through both direct and indirect pathways. We show that this wiring scheme confers increased selectivity. The biased stereotyped connectivity of the lateral horn contrasts with the probabilistic wiring of the mushroom body, reflecting the distinct roles of these regions in innate as compared to learned behaviors.

Most individual odor stimuli activate multiple odorant receptors and thus multiple types of olfactory receptor neurons. All the olfactory receptor neurons that express the same odorant receptor project to the same glomerulus in the brain, and so most individual stimuli are encoded by the combined activity of multiple glomeruli^{1–3}. As a consequence, higher-order neurons must combine signals across glomeruli to extract information about olfactory features of the environment. To understand higher olfactory processing, it is therefore fundamental to understand how signals from different glomeruli are combined.

In *D. melanogaster* and other insects, there are two higher-order olfactory brain regions—the lateral horn and the mushroom body. The lateral horn has been proposed to be analogous to the vertebrate amygdala, which receives a major olfactory projection from the olfactory bulb^{4–6}. The lateral horn likely holds the key to many olfactory behaviors in *Drosophila*. In particular, it is sufficient to mediate behavioral responses to odors that do not involve learned associations^{3,7,8}, and it receives the majority of glomerular projections^{9,10}.

Nevertheless, little is known about how odors are encoded in the lateral horn or how LHNs might integrate information across glomeruli. Individual olfactory glomeruli are known to send projections to stereotyped subregions of the lateral horn^{11–13}, but it is not known whether connectivity is stereotyped at the level of individual cells. A recent study described a cluster of LHNs in *Drosophila* that receives input from a single glomerulus and is devoted to the processing of pheromones¹⁴. This finding raises the possibility that each LHN is dedicated to a single glomerulus. At the other extreme, a study in locusts found that LHNs were broadly tuned to odors and on this basis suggested that individual neurons receive input from massive numbers of glomeruli¹⁵. A theoretical study proposed a third alternative: LHNs might add and subtract sparse, weighted inputs from coactivated glomeruli⁴. This latter study also suggested that some

combinations of glomeruli should be overrepresented, namely, glomeruli whose sum or difference represents a behaviorally useful computation.

By comparison, more is known about the connectivity of the mushroom body, which has been proposed to be analogous to the vertebrate piriform cortex^{4–6}. Individual mushroom body neurons combine input from sparse sets of glomeruli^{16,17}. These connections are regionally biased^{13,18}, and glomeruli with similar odor tuning tend to wire together¹⁹. However, connectivity appears to be probabilistic, and the pattern of glomerular inputs to the mushroom body seems to be different in different individuals^{11–13,16,20}. This finding is consistent with the conclusion that the mushroom body is involved in learned olfactory behaviors but not innate behaviors. Given the different roles of the mushroom body and lateral horn in olfactory behaviors, we might predict that these brain regions receive different patterns of connectivity from olfactory glomeruli and perform different sorts of computations on those glomerular inputs.

In this study we investigated connectivity and olfactory coding in the *Drosophila* lateral horn. Our results suggest a conceptual framework for understanding how this region integrates input from different glomeruli. Our results also show that there are distinctive differences in connectivity in the *Drosophila* higher-order brain regions that mediate innate as compared to learned olfactory behaviors.

RESULTS

Two morphological types of lateral horn projection neurons

To visualize all LHNs, we expressed photoactivatable GFP (PA-GFP) pan-neuronally and used two-photon excitation microscopy to activate PA-GFP throughout the lateral horn neuropil. As a consequence, activated PA-GFP labeled most of the neurons that have neurites in the lateral horn. We observed several large clusters of labeled somata. One cluster is dorsomedial to the lateral horn neuropil, and one

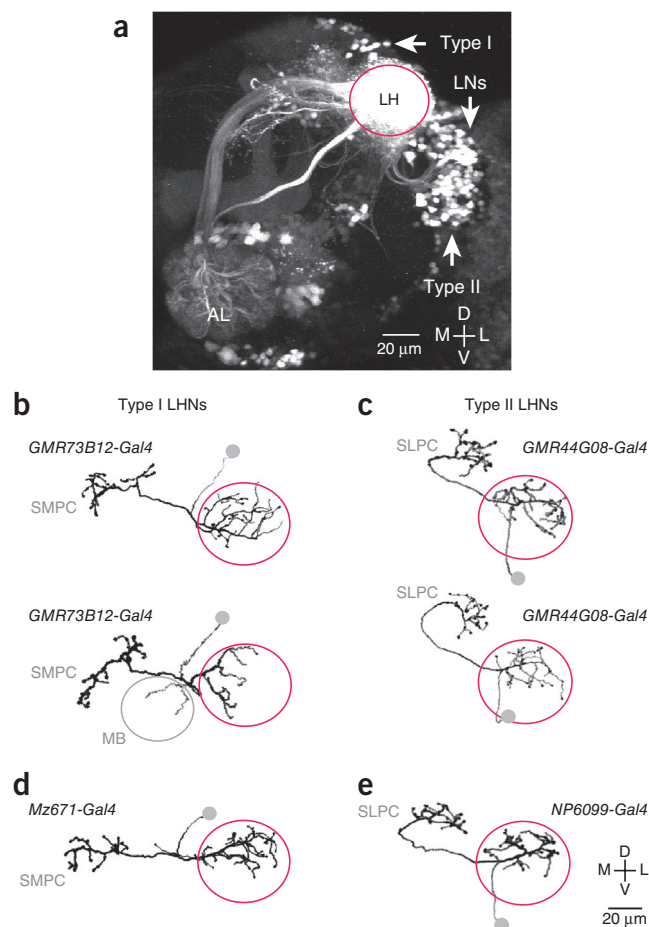
Department of Neurobiology, Harvard Medical School, Boston, Massachusetts, USA. Correspondence should be addressed to R.I.W. (rachel_wilson@hms.harvard.edu).

Received 17 September; accepted 27 November; published online 22 December 2013; doi:10.1038/nn.3613

Figure 1 Morphological types of lateral horn projection neurons. (a) Z projection of a coronal two-photon stack through a portion of the brain. PA-GFP is expressed pan-neuronally (under the control of *n-synaptobrevin-Gal4*) and photoconverted throughout the lateral horn (LH) neuropil. The magenta circle marks the boundary of the lateral horn. Arrows mark the three clusters of somata described in this study: type I neurons, type II neurons and lateral horn local neurons (LNs). The antennal lobe (AL) is weakly labeled because PN axons are photoconverted. Dorsal (D) is up, lateral (L) is right, medial (M) is left, and ventral (V) is down. Similar results were obtained in a total of four experiments. (b,c) Morphologies traced from biocytin-filled single neurons where the recorded neurons expressed GFP under the control of the indicated Gal4 lines. Somata were detached when the pipette was removed and are symbolized by gray circles. Type I neurons have dendrites in the lateral horn and project to the superior medial protocerebrum (SMPC). Type II neurons have dendrites in the lateral horn and project to the superior lateral protocerebrum (SLPC). Two examples are shown for each type. Morphologies similar to the examples shown here were observed in all neurons of a given type ($n = 8$ for each). In the type I fills, we noted minor variations across cells, including a small projection to the mushroom body (MB) calyx in two cases. (d,e) The morphologies of *Mz671* neurons (a subtype of type I) and *NP6099* neurons (a subtype of type II) were all essentially identical to the examples shown here ($n = 7$ and $n = 10$, respectively).

cluster is ventrolateral (Fig. 1a). Both clusters are connected to major neurite tracts that enter and exit the horn at distinctive locations. We define the neurons in these clusters as type I and type II neurons, respectively. Together these clusters comprise a substantial fraction of all labeled somata, although they do not encompass all morphological types¹⁸.

Through a visual screen of ~7,000 Gal4 enhancer trap lines²¹, we obtained two lines that label a large fraction of type I neurons, along with two lines that label a large fraction of type II neurons. We used these lines to drive GFP expression, and we filled a sample of GFP⁺ neurons with biocytin using *in vivo* whole-cell patch clamp recordings. These fills revealed that type I neurons all innervate the superior medial protocerebrum, although



they differ in their fine morphological structures. The same was true of type II neurons and the superior lateral protocerebrum (Fig. 1b,c and Online Methods).

Two enhancer trap lines have been identified previously that label small numbers of neurons with these morphologies. Specifically,

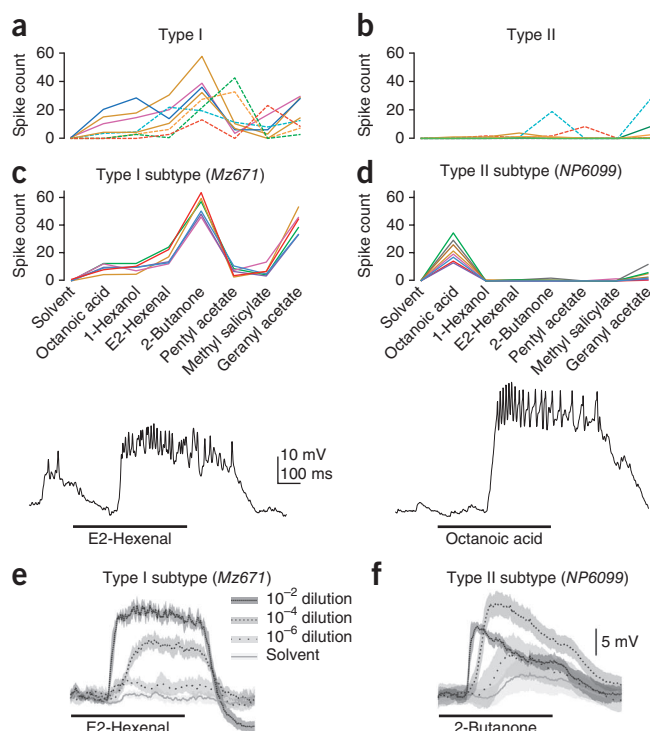
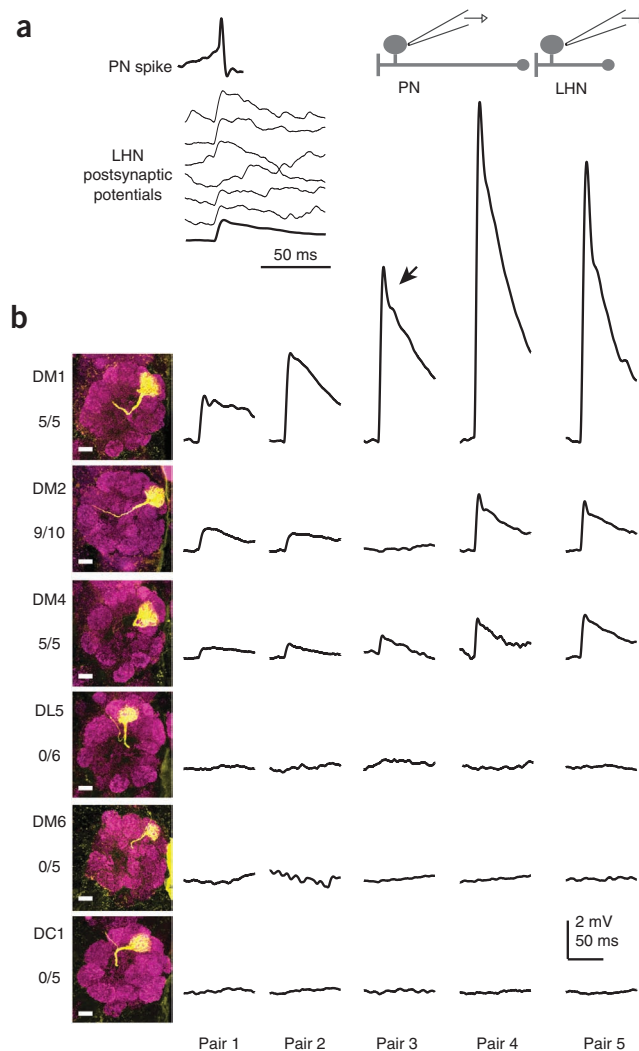


Figure 2 Odor selectivity in type I and type II neurons. (a) Odor selectivity in a population of type I neurons. Spikes are counted over a duration of 1 s starting at the odor-onset command. Each data point is the trial-averaged response to one odor in one experiment, with a line connecting all the responses from the same experiment ($n = 4$ from *GMR48F03-Gal4* (solid), and $n = 4$ from *GMR73B12-Gal4* (dashed)). All odors are 10^{-2} dilutions in paraffin oil (solvent), except where noted. Type I neurons have relatively broad tuning. (b) As in a but for a population of type II neurons ($n = 4$ from *GMR44G08-Gal4* (solid), and $n = 4$ from *GMR12H12-Gal4* (dashed); some neurons did not spike in response to any odor, but all neurons showed subthreshold responses). Tuning is significantly narrower in type II neurons as compared to type I neurons (unpaired two-tailed *t* test comparing lifetime sparseness (Online Methods), $P = 0.0014$, d.f. = 14).

(c) Within a subtype of type I neurons (labeled by *Mz671-Gal4*), odor selectivity is stereotyped ($n = 6$). The trace shows a typical *in vivo* whole-cell current clamp recording from one of these neurons. In all figures, a thick horizontal line indicates the 500-ms period when the odor valve was open. (d) As in c but for a subtype of type II neurons (labeled by *NP6099-Gal4*; $n = 8$). The trace shows a typical recording from one of these neurons. Tuning is significantly narrower in *NP6099* neurons as compared to *Mz671* neurons (unpaired two-tailed *t* test, $P = 1.9 \times 10^{-8}$, d.f. = 12). (e) Responses to an odor concentration series. Traces are averaged across trials and neurons (\pm s.e.m. across neurons). Responses are steady over time and grow monotonically with concentration. (f) As in e but for *NP6099* neurons ($n = 8$). Responses are more transient and are suppressed at high concentrations, suggesting the recruitment of inhibition.

Figure 3 Paired recordings identify convergent glomerular inputs.

(a) An example paired recording from a GFP⁺ *Mz671* neuron and one of its presynaptic PNs. The top trace is a single PN spike evoked by direct current injection. The bottom traces are postsynaptic membrane potentials in individual trials (the thicker line is the trial-averaged response). The vertical scale for the postsynaptic responses is the same as that in b. (b) Results from multiple experiments of this type. In these experiments, both the presynaptic and postsynaptic neurons were GFP⁺. A single row shows the trial-averaged postsynaptic responses from five paired recordings, each in a different brain. On the left are z projections of confocal stacks through the antennal lobe displaying the dendritic tufts of biocytin-filled PNs (scale bars, 10 μ m) together with the total number of connections observed and total number of pairs recorded. DM1 consistently evoked larger responses than either DM2 or DM4 (one-way analysis of variance (ANOVA), $F(2,16) = 12.45$, $P = 5.5 \times 10^{-4}$, followed by *post hoc* unpaired two-tailed *t* tests, DM1 compared to DM2: $P = 0.015$, d.f. = 12; DM1 compared to DM4: $P = 0.019$, d.f. = 8). Some responses have a transient peak (arrow), which likely reflects a contribution of voltage-gated postsynaptic conductances. Data are not shown for the following glomeruli, none of which were connected: VA4 (0/1), VC1 (0/3), VC2 (0/3), VL2A (0/1), VM2 (0/2) and VM7 (0/2).



Mz671-Gal4 labels three type I neurons on each side of the brain, and *NP6099-Gal4* labels three type II neurons^{13,18}. We used single-cell biocytin fills to confirm these morphologies (Fig. 1d,e). These lines provide genetic access to small, genetically defined subtypes of neurons belonging to each major type.

Odor selectivity in type I and type II neurons

We next surveyed the odor responses of the type I and type II populations using the *Gal4* lines that drive expression in large numbers of neurons within each type to label these neurons with GFP. We made *in vivo* whole-cell patch clamp recordings from a sample of GFP⁺ neurons within each line. We used a test panel of chemically diverse odors in these experiments to coarsely sample odor space. Because these *Gal4* lines label many cells, we expected the labeled cells to exhibit diverse odor preferences. Indeed, within each morphological type, we found that different neurons had different preferred odors (Fig. 2a,b). Notably, we found a systematic and significant difference between the odor tuning of type I and type II neurons: the former were broadly tuned, whereas the latter were more selective.

We then focused specifically on the small numbers of type I and type II neurons defined by *Mz671-Gal4* (referred to as *Mz671* neurons) and *NP6099-Gal4* (referred to as *NP6099* neurons). We found that all three of the *Mz671* neurons showed stereotyped odor responses, both within brains and across brains. Similarly to most type I neurons, they were broadly tuned (Fig. 2c).

NP6099 neurons also showed stereotyped odor responses, both within and across brains. Similarly to most type II neurons, they were narrowly tuned (Fig. 2d). Thus, the morphologies of both *Mz671* and *NP6099* neurons accurately predicted their tuning breadth.

In addition, we noticed differences in the concentration tuning of these neurons. The responses of *Mz671* neurons grew monotonically over a large dynamic range of concentrations. By contrast, the responses of *NP6099* neurons were suppressed, and also became more transient, at high concentrations (Fig. 2e,f). This result suggests that some of the odor responses of *NP6099* neurons might be suppressed by inhibition.

In sum, these results show that type I and type II neurons differ systematically in the breadth of their odor tuning. The *Mz671* and *NP6099* neurons are exemplars of each type. To understand the

connectivity that underlies the odor responses of LHNs of each type, we focused on *Mz671* and *NP6099* neurons.

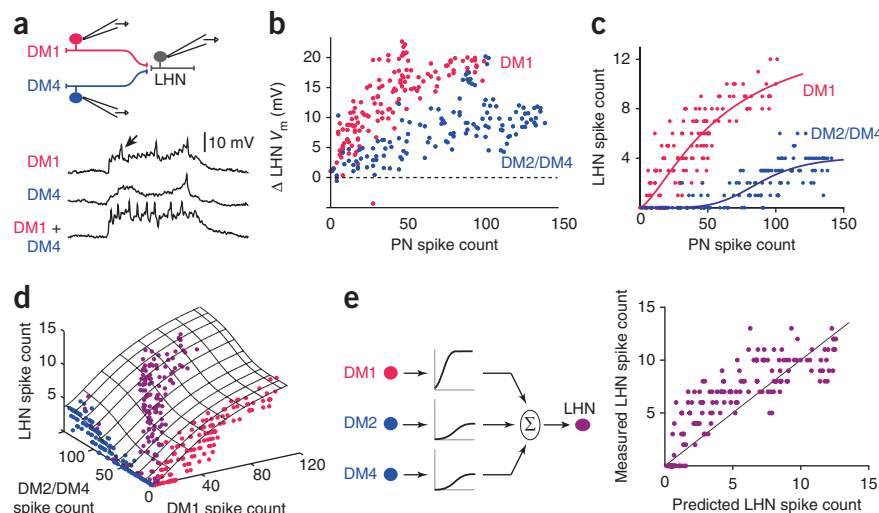
Connectivity from glomeruli to type I neurons

We next screened for connections from antennal lobe projection neurons (PNs) onto LHNs using paired *in vivo* whole-cell patch clamp recordings and focusing initially on the *Mz671* population. In every experiment, we targeted one electrode to one *Mz671* neuron and one randomly selected PN, depolarizing each PN with injection of direct current so that it fired one spike per trial. In most cases, the cells were not connected. In a small minority of pairs, we observed excitatory postsynaptic potentials with short and consistent latencies (<1.5 ms), which is indicative of monosynaptic connections (Fig. 3a). In these cases, we filled the PN with biocytin for *post hoc* identification.

In this screen, we performed 120 separate paired recordings and obtained five connected pairs. All the PNs in these pairs innervated one of three glomeruli (DM2, DM4 or VA7l). This connection rate implies that the *Mz671* neurons receive input from only a handful of glomeruli, nominally four or fewer glomeruli if we assume unbiased sampling (Discussion).

To determine whether the connections are stereotyped, we performed paired recordings in which we labeled antennal lobe PNs with GFP rather than randomly selecting them. We selectively targeted PNs in 12 glomeruli: 2 that emerged from our screen (DM2 and DM4)

Figure 4 Summing excitatory input from multiple glomeruli. (a) A *Mz671* neuron and two of its presynaptic PNs are labeled with GFP and recorded simultaneously. In interleaved trials, the PNs are driven to fire either alone or together (using 500-ms steps of depolarizing current injected through the patch pipettes), and the responses of the LHN are recorded. The postsynaptic membrane potential is shown for three trials (the arrow indicates a spike). The saw-tooth fluctuations (visible especially when DM1 is spiking) reflect large unitary postsynaptic potentials that time lock to individual PN spikes. The voltage traces shown are 1 s in duration. (b) Relationship between PN spike count and LHN membrane potential (V_m), where the two PNs are each stimulated in separate trials. Magenta points are from trials in which DM1 PNs were stimulated, and blue points are from trials in which either DM2 or DM4 (DM2/DM4) PNs were stimulated, depending on the experiment (three experiments in total). DM2 and DM4 connections had similar strength, and so we pooled the data from these glomeruli. (c) Relationship between PN spike count and LHN spike count, where the two PNs are each stimulated in separate trials. The fits are sigmoid functions. (d) Data from all trials, including trials in which the two PNs were stimulated separately (magenta and blue) and trials in which they were stimulated simultaneously (purple). The hatched surface is a fit to the model. (e) Left, model schematic. Spike rates from each glomerulus are passed through an input-specific saturating nonlinearity and then summed to generate the LHN firing rate. The input-specific nonlinearities are first fit to data from a single PN, and then these same nonlinearities are used to generate the prediction for trials in which both PNs were stimulated simultaneously. Right, measured LHN spike counts versus the spike counts predicted by the model. Each point represents a different trial in which both PNs were stimulated simultaneously.



plus 10 others (DC1, DL5, DM1, DM6, VA4, VC1, VC2, VL2A, VM2 and VM7). We filled all PNs recorded in this data set with biocytin to confirm their identity.

These experiments showed that the connectivity from PNs to *Mz671* neurons was invariant. Three glomeruli were always or almost always connected (DM1, DM2 and DM4), and the other ten glomeruli were never connected (Fig. 3b). Notably, a stereotyped synaptic weight was associated with each connected glomerulus: DM1 consistently evoked larger synaptic responses than either DM2 or DM4.

Summing excitatory input from multiple glomeruli

Three glomeruli that provide input to *Mz671* neurons (DM1, DM2 and DM4) are coactivated by many fruity-smelling organic acetates^{22,23}. Therefore, some salient olfactory stimuli (such as fruits) might coactivate these glomeruli. To determine how signals from coactivated glomeruli are integrated in these LHNs, we labeled one *Mz671* neuron and two of its presynaptic PNs with GFP, and we made simultaneous triple *in vivo* recordings from these neurons. We depolarized the two PNs with current injection so that they fired trains of spikes, either individually or together (Fig. 4a).

These experiments revealed that postsynaptic spiking could be driven by a single PN. When PNs spiked at high rates, either individually or simultaneously, the postsynaptic response followed a saturating sigmoid function (Fig. 4b,c). Because input from different PNs saturated at different levels, the mechanism of saturation likely resides at the synapse and not the process of spike generation in the postsynaptic neuron.

In trials in which we stimulated both PNs, the postsynaptic response was accurately predicted by summing the responses to each input alone (Fig. 4d,e). The prediction was generated by fitting sigmoid functions to the trials in which we stimulated single PNs individually and then simply summing the predicted postsynaptic responses to each PN input. This model provided a reasonably good fit to the data ($R^2 = 0.69$; Fig. 4e and Online Methods). However, the model systematically underestimated postsynaptic responses to relatively

weak presynaptic inputs. In these cases, one input was often too weak to elicit postsynaptic spikes when stimulated alone but was strong enough to modestly increase postsynaptic spike rates when coactivated with the second input. Thus, the inputs to the *Mz671* neurons sum in a fairly linear manner, although they elicit modestly supralinear postsynaptic responses at weak presynaptic firing rates.

These triple recordings show that a single glomerulus can be sufficient to drive spikes in an LHN and that recruitment of additional presynaptic glomeruli causes LHN responses to increase further. On the basis of these results, we predict that LHN odor responses can be driven by odor-evoked spiking in a single presynaptic glomerulus. We also predict that LHN odor responses should increase as additional glomeruli are recruited by an odor stimulus. Summing over glomeruli in this manner could allow LHNs to be sensitive to a broader range of stimuli than any single one of their input glomeruli.

To test these predictions directly, we recorded the odor responses of *Mz671* neurons, DM4 PNs and DM1 PNs. We focused on one odor (methyl acetate) diluted over a large range of concentrations. We chose this odor because it activates both DM4 and DM1 PNs, but it activates them at different concentrations; in addition, this odor is selective for DM4 at low concentrations (Online Methods). As such, this odor allowed us to test the specific predictions emerging from our triple recordings. We found that the *Mz671* neurons were recruited by low concentrations of this odor that are selective for glomerulus DM4 (Fig. 5a,b). This finding confirms that odor responses in a single presynaptic glomerulus are sufficient to drive these neurons. When we increased the odor concentration, DM4 PNs were saturated, and DM1 PNs were recruited. LHN responses were sensitive to the recruitment of DM1 PNs: their responses continued to grow even though input from DM4 was no longer growing (Fig. 5a,b). This result confirms that odor responses in *Mz671* neurons increase as additional glomeruli are recruited by an odor.

Notably, *Mz671* neurons encode a broader range of concentrations as compared to their individual presynaptic PNs. We quantified this observation by measuring the steepness of the concentration-response

Figure 5 LHN odor responses are sensitive to single glomeruli. (a) Typical *in vivo* whole-cell recordings from a *Mz671* neuron, a DM1 PN and a DM4 PN (recorded separately). The odor used is methyl acetate. Low concentrations recruit DM4 but not DM1. High concentrations saturate DM4 and begin recruiting DM1. LHN responses increase over the entire concentration range. (b) Concentration-response functions. Different points at a single concentration are from different experiments ($n = 6$ for each cell type). Smooth lines are fits to the equation

$$f([\text{odor}]) = A \frac{1}{1 + \sigma^n / [\text{odor}]^n}$$

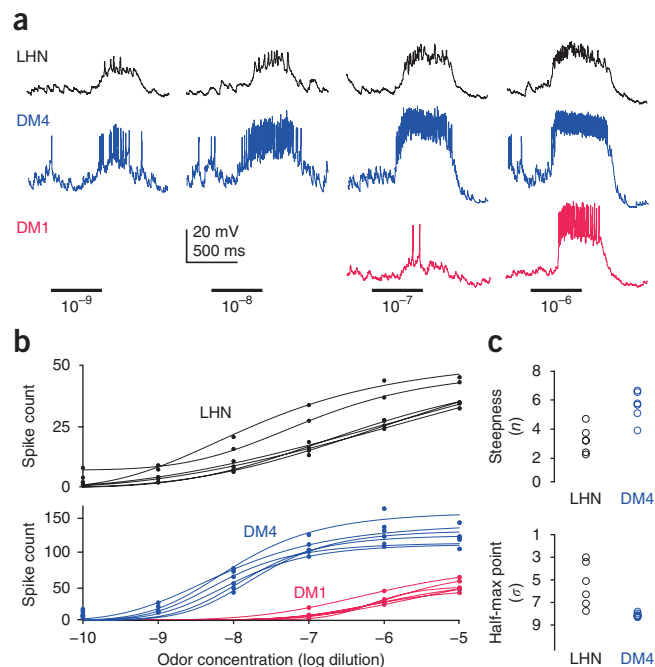
where [odor] is the log odor concentration and A is a constant. (c) The fitted parameters that describe the shape of the curve (n and σ) are significantly different for DM4 PNs and LHNs (unpaired two-tailed t tests, n : $P = 0.0017$, d.f. = 10; σ : $P = 0.0076$, d.f. = 10). The parameter n measures the steepness of the curve, and σ is the concentration that produces a half-maximal (half-max) LHN response (in units of $-\log$ dilution). The discrepancy between the spike counts shown in **b** and **Figure 4** is addressed in **Supplementary Figure 1**.

functions; this analysis showed that the LHN responses are significantly less steep (**Fig. 5c**). This finding arises from the fact that the PNs in question are sensitive to different ranges of concentration of the same odor. As a result, summing the two PN responses produces a broader dynamic range in the postsynaptic LHNs. The PN concentration-response functions are steeper than those of LHNs over a relatively limited portion of the odor concentration range. In addition, the trial-to-trial reliability of PN responses is similar to that of LHN responses for matched odor-evoked firing rates (data not shown). Thus, PNs are more informative about concentration over a narrow range, but LHNs carry information about a broader range.

Connectivity from glomeruli to type II neurons

Next we investigated connectivity onto the *NP6099* (type II) neurons. Overall, type II neurons are more narrowly tuned than are type I neurons (**Fig. 2**), suggesting that they receive excitation from fewer glomeruli. Indeed, we found 0 connections in 82 paired recordings from randomly selected PNs and *NP6099* neurons. As there are only 49 glomeruli in total, this connection rate raises the possibility that the *NP6099* neurons receive PN input from only one glomerulus.

A previous study predicted that *NP6099* neurons receive direct input from glomeruli DP1m and VA2, as their dendrites overlap with the projections from these glomeruli¹³. Because there is no Gal4 line available that is selective for the PNs in either of these glomeruli, we used an alternative approach to target these PNs for paired recordings (**Fig. 6**). Namely, we expressed PA-GFP under the control of



a Gal4 line that is expressed in many PNs, and we photoactivated the glomerulus of interest specifically. This allowed us to target our electrodes selectively to PNs in either DP1m or VA2. We filled each recorded PN to confirm its identity *post hoc*.

Using this approach, we performed four paired recordings with DP1m PNs and *NP6099* neurons. In all four cases, we found a connection. By contrast, we observed no connection with glomerulus VA2 in six of seven experiments, although there was a weak connection in one experiment (**Fig. 6**). This example suggests that there are small variations in the wiring of connections from PNs onto LHNs, perhaps because of developmental errors (another example is the 'missing' connection from a DM2 PN in **Fig. 3b**). Nonetheless, the overall conclusion from these recordings is that connectivity is highly stereotyped. In particular, it is notable that the VA2 PNs do not form connections with the *NP6099* neurons, although their axons and dendrites exhibit considerable overlap¹³.

Gating of feedforward excitation in type II neurons

Identifying presynaptic antennal lobe PNs for the *NP6099* neurons allowed us to compare the odor tuning of these synaptically connected PNs and LHNs. We found that every test odor that activated the LHNs also activated the DP1m PNs (**Fig. 7a,b**). This finding is consistent with the idea that the *NP6099* neurons receive most or all of their excitation from DP1m. In further support of this idea, we found that the input from DP1m is strong enough to account for the size of the excitatory odor responses in the LHN. Specifically, in paired recordings, injection of direct current into DP1m PNs elicited an LHN response that matched the strongest odor-evoked

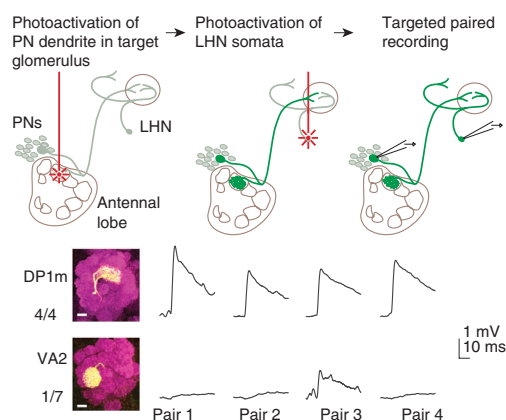
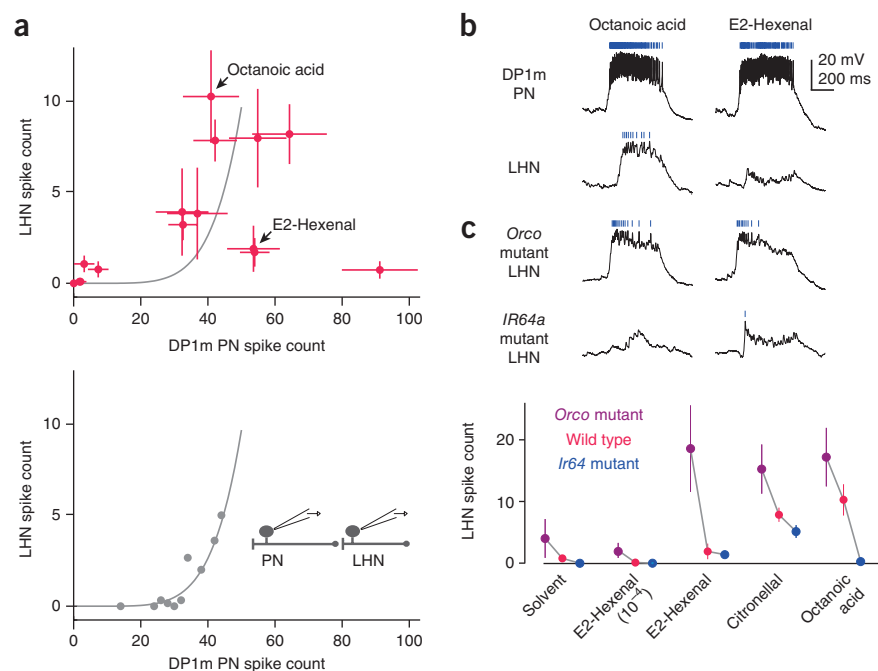


Figure 6 Paired recordings identify excitation from one glomerulus. Top, paired *in vivo* recordings guided by PA-GFP. PA-GFP was expressed in many PNs (under the control of *GH146-Gal4*) and in *NP6099* neurons. We photoactivated a single glomerulus (either DP1m or VA2) to label the corresponding PN soma. We next photoactivated the *NP6099* neuron somata and then simultaneously recorded from a PN and an LHN. Bottom, results from multiple experiments of this type (**Fig. 3b**). Four of four DP1m pairs showed a connection. Only one of seven VA2 pairs showed a connection, and this response was unusually weak.

Figure 7 Odor-selective inhibition gates excitation from glomerulus DP1m. **(a)** Odor responses of *NP6099* neurons plotted against responses of DP1m PNs. Each point represents an odor stimulus (mean \pm s.e.m. computed across experiments, $n = 4$ –13 PNs and $n = 4$ –17 LHNs per point; the odors are shown in **Supplementary Fig. 2**). The bottom plot shows data from a separate set of experiments (paired recordings from DP1m PNs and *NP6099* neurons) in which the PN was directly depolarized to fire trains of spikes using current injection through the patch pipette ($n = 2$ pairs, pooled trials binned by PN spike rate, averaged within a bin and fit with an exponential). These paired recordings show that synaptic excitation from DP1m is strong enough to account for the strongest odor responses of *NP6099* neurons (the gray fitted function in the top plot is reproduced from the bottom plot). **(b)** Odor responses of DP1m PNs and *NP6099* neurons to octanoic acid and E2-hexenal (both 10^{-2} dilution). The rasters above each trace show spikes. Although these two stimuli elicit similarly strong responses in DP1m PNs, the postsynaptic response to E2-hexenal is selectively suppressed. **(c)** Both responses are disinhibited by the *Orco* mutation (which also eliminates the difference between the responses) and attenuated by the *Ir64a* mutation. The bottom plot shows quantification of responses to several stimuli in wild-type flies, *Orco* mutants and *Ir64a* mutants (mean \pm s.e.m.). For both genotypes, the effect across all odors was significant ($n = 4$ –6 experiments per odor for each mutant and $n = 9$ –17 experiments per odor for wild-type flies; two-way ANOVA, $F_{Ir64a}(1,77) = 9.25$, $P = 0.0032$; $F_{Orco}(1,71) = 719.43$, $P = 3.63 \times 10^{-5}$).



response to the same odor-evoked PN firing rate (**Fig. 7a**). Thus, DP1m may be the only glomerulus that provides direct excitatory input to *NP6099* neurons.

Notably, some odors elicited a robust response in DP1m PNs but little or no postsynaptic spiking in the *NP6099* neurons. This result suggests that excitatory input from DP1m is gated by strong, odor-selective inhibition from coactivated glomeruli. For example, whereas both octanoic acid and E2-hexenal elicited a robust PN response, only octanoic acid elicited a response in the LHNs (**Fig. 7a,b**). This finding suggests that there is a glomerulus that is activated by E2-hexenal but not octanoic acid, and inhibition from this glomerulus gates the excitation arising from DP1m. Because inhibition is tuned, it likely arises from a small number of glomeruli rather than the summed activity of many glomeruli (**Supplementary Fig. 2**).

To explore the origins of inhibition further, we recorded from these same LHNs in *Orco* mutants. The *Orco* gene encodes a co-receptor that is expressed by most olfactory receptor neurons²⁴. Many olfactory receptor neurons are *Orco* positive, and in these neurons, *Orco* is absolutely required for olfactory transduction²⁴. However, DP1m olfactory receptor neurons do not require *Orco* for normal transduction²⁵. We found that the *Orco* mutation disinhibited odor responses in the *NP6099* neurons (**Fig. 7c**). This result indicates that one or more *Orco*-positive glomeruli are the source of inhibition in these LHNs.

Conversely, odor responses in *NP6099* neurons were reduced by a mutation in *Ir64a*. The *Ir64a* gene encodes an odorant receptor that is expressed by DP1m olfactory receptor neurons and is necessary for their normal function²⁶. This mutation does not completely abolish odor responses in the DP1m olfactory receptor neurons (G. Suh, personal communication), and so the residual odor responses we observed in the mutant are compatible with the conclusion that DP1m is the only source of direct excitation to the *NP6099* neurons.

Together these two mutations indicate that odor-specific inhibition from *Orco*-positive glomeruli gates excitation from glomerulus DP1m.

Which inhibitory neurons relay odor-specific inhibition to these LHNs? Likely candidates are the GABAergic inhibitory antennal lobe PNs (iPNs)^{10,27,28}. These PNs project through an axon tract that is separate from the tract carrying the axons of excitatory PNs (ePNs), so we were able to use two-photon laser transection to selectively cut the axons of ePNs, leaving the iPN axons intact (**Fig. 8a**). This manipulation abolished excitation in the *NP6099* neurons, revealing pure inhibition (**Fig. 8b**). This residual inhibition likely originated from iPNs, as it disappeared when we cut both the iPN and ePN axon tracts (**Fig. 8b**). However, this residual inhibition was weak, and when we cut the axons of iPNs rather than the axons of ePNs, we observed little to no disinhibition (**Fig. 8b,c**), especially as compared to the effects of the *Orco* mutation (**Fig. 7c**).

Together these results imply a second source of inhibition in addition to the inhibition arising from iPNs. The logical candidates are GABAergic neurons in the lateral horn itself (**Fig. 8a**). Therefore, we performed a GABA immunostain and found a cluster of GABAergic somata adjacent to the lateral horn (**Supplementary Fig. 3**). We identified a Gal4 line that labels these neurons, and we patched and filled individual labeled cells from this line. This method confirmed that these neurons have purely local arbors (**Fig. 8d**). Notably, we observed that all the neurons we recorded from had narrow odor tuning (**Fig. 8e–g**). Thus, these local neurons are well positioned to provide odor-specific inhibition.

In sum, these results provide evidence that inhibition arises from two sources. Some inhibition arises from a direct GABAergic projection from the antennal lobe, and additional inhibition arises from a local GABAergic circuit within the lateral horn. Although inhibition is much more prominent in type II neurons, it can occasionally be seen in type I neurons as well (**Supplementary Fig. 4**).

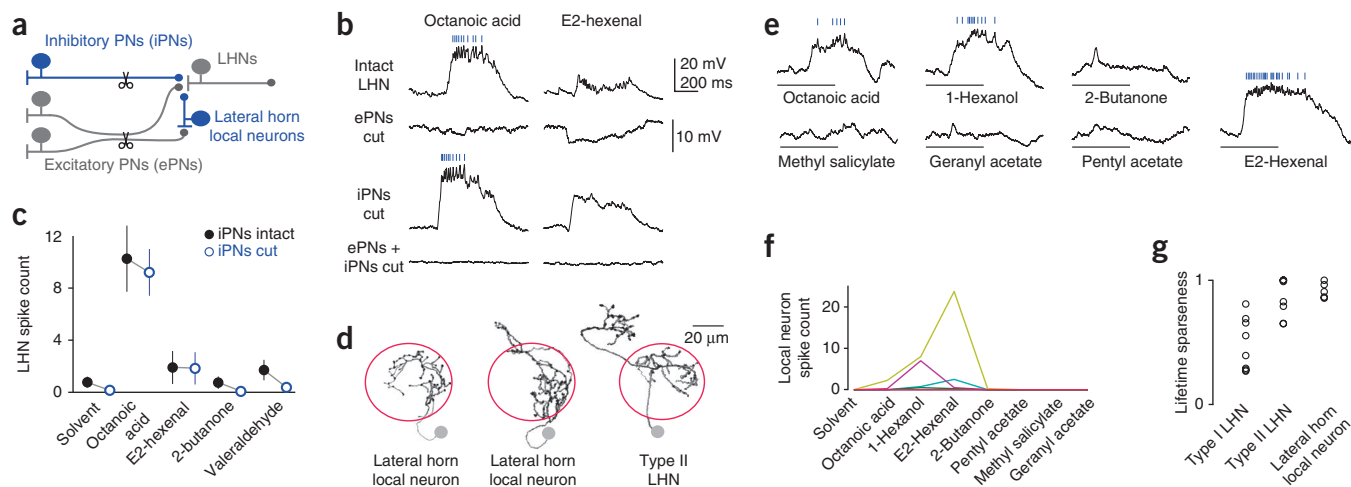


Figure 8 Circuit origin of inhibition. (a) Two inhibitory circuits, one through GABAergic iPNs in the antennal lobe and another through GABAergic local neurons in the lateral horn. The axon tracts of iPNs and ePNs are segregated and can therefore be cut selectively. (b) Odor responses of DP1m PNs and *NP6099* neurons (the top trace is reproduced from Fig. 7b). Cutting ePN axons eliminates excitation and reveals inhibition (cells were held at a depolarized potential to better show inhibition; there is a different vertical scale in this row; similar results were obtained in nine experiments). However, cutting iPN axons does not completely abolish inhibition (compare with the *Orco* mutation in Fig. 7c). Cutting both tracts eliminates all odor responses. (c) Odor responses of *NP6099* neurons in experiments in which iPNs were intact (data from Fig. 7) or cut ($n = 6$; mean \pm s.e.m.). There is no significant effect on spike counts (two-way ANOVA, $F_{1,67} = 0.45$, $P = 0.51$), although subthreshold responses were often partially disinhibited. (d) Sample morphologies of lateral horn local neurons traced from biocytin fills. These neurons are immunopositive for GABA (Supplementary Fig. 3). Similar fills were obtained for a total of seven cells. A few of these neurons have local arbors that extend beyond the boundaries of the lateral horn (for example, the middle neuron). The morphology of a type II LHN is shown for comparison (reproduced from Fig. 1). (e) Odor responses of a GABAergic lateral horn local neuron. The scale is the same as that in b. (f) Odor selectivity of a population of lateral horn local neurons. Spikes are counted over a duration of 1 s starting at the odor-onset command. Each line connects spike counts from the same neuron ($n = 7$; some cells do not spike in response to any odors, but all cells displayed subthreshold responses). (g) Lifetime sparseness of odor-evoked spike rates in type I and type II neurons (the same cells as those in Fig. 2a,b) and lateral horn LNs ($n = 5$ cells, the same cells as those in f except that here the cells that did not spike in response to either current injection or odor are omitted). Each symbol represents a different experiment. A sparseness of 1 is maximally selective, and 0 is nonselective. One LN and one type II neuron spiked in response to current injection but not odor and were assigned a sparseness of 1. The spiking responses of lateral horn LNs are highly selective.

DISCUSSION

Glomerular connections to LHNs

To understand higher olfactory processing, it is fundamentally important to know how many glomeruli provide input to a typical higher-order neuron. It is also important to know whether these connections are stereotyped, whether different glomerular inputs are associated with different synaptic weights and whether some combinations of glomeruli occur preferentially. In this study we used paired recordings to map the connectivity of representative LHN projection neurons and to address these questions. Because we found that connectivity is stereotyped, we could use large numbers of paired recordings to build a cumulative picture of the connectivity of these neurons.

Our random samples of PN-LHN pairs allowed us to estimate the number of input glomeruli for each LHN type. For our representative type I neurons (*Mz671* neurons), we performed 120 paired recordings with random PNs and found five connections. Given 49 glomeruli²⁹, binomial statistics would indicate with ~95% confidence that there are at most four connected glomeruli. Indeed, we identified four inputs for these neurons (DM1, DM2, DM4 and VA7l). This calculation assumes that there are equal numbers of PNs in all glomeruli. In total, there are ~150 PNs³⁰, which would predict three PNs per glomerulus, but it is known that some glomeruli contain more than three PNs (for example, glomerulus DA1 (ref. 31)) and some contain only one PN³². If a glomerulus contained only one PN, then we would be more likely to miss it, and indeed, glomerulus DM1 was a near miss: it contains one PN³², and it did not turn up in our random screen. We identified DM1 only as a result of our targeted paired recordings. Thus, four

glomeruli might be an underestimate. Nonetheless, it seems likely that each type I neuron receives input from fewer than ten glomeruli.

For our representative type II neurons (*NP6099* neurons), we performed 82 paired recordings with random PNs and found 0 connections. Binomial statistics would indicate that there are at most two connected glomeruli, with the same caveats as those listed above. However, for these neurons, there is independent evidence arguing that DP1m is the only excitatory input. Specifically, all the odors that activate these neurons also activate DP1m PNs, and the firing rates of DP1m PNs are sufficient to predict the strongest odor responses in these neurons. It will be interesting to learn whether all type II neurons receive excitatory input from a single glomerulus. It is notable that VA2 PNs do not connect to these neurons despite substantial axon-dendrite overlap¹³. These results raise the question of how an LHN reliably forms a connection with one axon but avoids forming a connection with another axon in a case where the two axons are overlapping.

A notable conclusion of our study is that some glomerular combinations are substantially over-represented in the lateral horn. Consider the fact that there are three *Mz671* neurons per lateral horn, but there are only several hundred LHNs in total (on the basis of cell counts in experiments in which we expressed PA-GFP pan-neuronally and photoactivated a large volume of the lateral horn; Fig. 1a). We identified four glomeruli connected to *Mz671* neurons. Given that there are 49 glomeruli in total²⁹, there are >200,000 possible combinations of four glomeruli. This is far larger than the total number of neurons in the lateral horn. Moreover, the particular glomerular combination sampled by the *Mz671* neurons occurs not once but at least three times

in every lateral horn. Therefore, the space of possible glomerular combinations is sampled nonrandomly.

Our paired recordings also showed that different glomerular inputs to an LHN can be associated with nonuniform and stereotyped synaptic weights. This idea has been proposed previously as a way to render LHNs more selective for a particular olfactory feature⁴. This result also indicates a high level of precision in the development of this circuit.

In many of these respects, our results show that the lateral horn differs radically from the mushroom body, which is the other third-order olfactory region in insects. In the mushroom body, the pattern of glomerular inputs appears to be different in different individuals^{11–13,16,20}. And although there are regional biases in connections from glomeruli to the mushroom body^{18,33}, and glomeruli with similar tuning tend to wire together¹⁹, connectivity in the mushroom body nonetheless seems to be probabilistic rather than deterministic. This contrasts with the highly stereotyped wiring we found in the lateral horn. Disrupting the mushroom body impairs learned but not unlearned olfactory discriminations, implying that the lateral horn is sufficient for innate olfactory behavior^{7,8}. Thus, the mushroom body and lateral horn serve different behavioral functions, and our results demonstrate that they also sample differently from olfactory glomeruli.

It should be noted that the stereotypy we observed may be specified entirely by the genetic inheritance of these organisms, but this is not necessarily the case. We raised all the flies in our experiments in a similar environment. Future studies will be needed to determine whether there is any experience-dependent element in these connections or their weights.

Odor coding and computations in LHNs

Our results demonstrate that different types of LHNs carry out distinct computations on the information they receive from olfactory glomeruli. Type I neurons are broadly tuned to odors, and *Mz671* neurons are typical of type I neurons in this respect. Consonant with this, we found that *Mz671* neurons pool excitation from a handful of coactivated glomeruli, and input from even a single glomerulus can be sufficient to drive postsynaptic spiking. For this reason, we might expect these LHNs to be more broadly tuned to odors than are PNs. Broad odor tuning to a group of related chemicals might be a useful way to link a large region of chemical space (for example, odors associated with fruit) with an innate behavioral program (for example, feeding).

In addition, we observed that the *Mz671* neurons have a broader dynamic range for concentration encoding as compared to their presynaptic PNs. *Drosophila* can generalize across different concentrations of the same odor, and this behavioral performance requires integrating activity across multiple glomeruli that are coactivated by some odors but with different sensitivities to those odors^{34,35}. Whereas each individual glomerulus can only encode concentration over roughly two orders of magnitude, summing several glomeruli that have different dynamic ranges can yield a broader range of sensitivity³⁴. This is precisely what the *Mz671* neurons do. Thus, type I LHNs might have a role in concentration generalization.

In contrast to type I neurons, type II neurons are narrowly tuned, and *NP6099* neurons are typical of type II neurons in this respect. Again, consonant with their narrow tuning, we showed that *NP6099* neurons combine excitation from one (or a few) glomeruli with tuned inhibition from coactivated glomeruli, yielding greater selectivity. This computation is distinct from that performed by the *Mz671* neurons. On theoretical grounds, combining excitation and inhibition from coactivated glomeruli has been proposed as a way to generate

selectivity⁴. Behavioral data show that *Drosophila* can perform fine discriminations among odor stimuli with different chemical compositions^{34,36}. Neurons with high selectivity might be a useful way to link specific odor stimuli with behavioral programs.

In other sensory systems, the receptive field of a neuron can be described as a set of positive and negative weights over stimulus space³⁷ or neural space³⁸. Here we show that this framework can be extended to higher-order olfactory receptive fields, which are essentially a set of positive and negative weights over olfactory glomeruli. Each glomerulus corresponds to an odorant receptor, and each receptor is selective for a molecular feature¹. Thus, higher-order olfactory receptive fields represent weighted sums of molecular features. In other sensory systems, receptive field structures are nonrandom insofar as they have a strong tendency to sample from overlapping regions of stimulus space, reflecting the statistical regularities of the environment³⁹. Analogous to this, we described neurons that sample from glomeruli with overlapping chemical tuning, and we showed that the sampling is highly nonrandom. It will be interesting to investigate how the computations that occur in the lateral horn might relate to the statistical distribution of odors in the environment, as well as their ecological relevance to the organism.

METHODS

Methods and any associated references are available in the [online version of the paper](#).

Note: Any Supplementary Information and Source Data files are available in the online version of the paper.

ACKNOWLEDGMENTS

We are grateful to G. Technau (Johannes Gutenberg University Mainz) for the gift of *Mz671-Gal4*, J. Simpson (Janelia Farm Research Campus) for *c315a-Gal4*, G. Rubin and B. Pfeiffer (Janelia Farm Research Campus) for *pJFRC7-20XUAS-IVS-mCD8::GFP(attP40)* and S.R. Datta (Harvard Medical School) for *UAS-C3PA-GFP* and *UAS-SPA-GFP*. We thank members of the Wilson laboratory for comments on the manuscript. This work was supported by a research project grant from the US National Institutes of Health (R01DC008174). R.I.W. is a Howard Hughes Medical Institute Investigator. M.F. was supported in part by a Howard Hughes Medical Institute International Student Research Fellowship.

AUTHOR CONTRIBUTIONS

M.F. and R.I.W. designed the experiments. M.F. performed the experiments and analyzed the data. M.F. and R.I.W. wrote the manuscript.

COMPETING FINANCIAL INTERESTS

The authors declare no competing financial interests.

Reprints and permissions information is available online at <http://www.nature.com/reprints/index.html>.

1. Bargmann, C.I. Comparative chemosensation from receptors to ecology. *Nature* **444**, 295–301 (2006).
2. Vosshall, L.B. & Stocker, R.F. Molecular architecture of smell and taste in *Drosophila*. *Annu. Rev. Neurosci.* **30**, 505–533 (2007).
3. Masse, N.Y., Turner, G.C. & Jefferis, G.S. Olfactory information processing in *Drosophila*. *Curr. Biol.* **19**, R700–R713 (2009).
4. Luo, S.X., Axel, R. & Abbott, L.F. Generating sparse and selective third-order responses in the olfactory system of the fly. *Proc. Natl. Acad. Sci. USA* **107**, 10713–10718 (2010).
5. Miyamichi, K. *et al.* Cortical representations of olfactory input by trans-synaptic tracing. *Nature* **472**, 191–196 (2011).
6. Sosulski, D.L., Bloom, M.L., Cutforth, T., Axel, R. & Datta, S.R. Distinct representations of olfactory information in different cortical centres. *Nature* **472**, 213–216 (2011).
7. de Belle, J.S. & Heisenberg, M. Associative odor learning in *Drosophila* abolished by chemical ablation of mushroom bodies. *Science* **263**, 692–695 (1994).
8. Connolly, J.B. *et al.* Associative learning disrupted by impaired Gs signaling in *Drosophila* mushroom bodies. *Science* **274**, 2104–2107 (1996).
9. Stocker, R.F. The organization of the chemosensory system in *Drosophila melanogaster*: a review. *Cell Tissue Res.* **275**, 3–26 (1994).

10. Tanaka, N.K., Endo, K. & Ito, K. Organization of antennal lobe-associated neurons in adult *Drosophila melanogaster* brain. *J. Comp. Neurol.* **520**, 4067–4130 (2012).
11. Marin, E.C., Jefferis, G.S., Komiyama, T., Zhu, H. & Luo, L. Representation of the glomerular olfactory map in the *Drosophila* brain. *Cell* **109**, 243–255 (2002).
12. Wong, A.M., Wang, J.W. & Axel, R. Spatial representation of the glomerular map in the *Drosophila* protocerebrum. *Cell* **109**, 229–241 (2002).
13. Jefferis, G.S. *et al.* Comprehensive maps of *Drosophila* higher olfactory centers: spatially segregated fruit and pheromone representation. *Cell* **128**, 1187–1203 (2007).
14. Ruta, V. *et al.* A dimorphic pheromone circuit in *Drosophila* from sensory input to descending output. *Nature* **468**, 686–690 (2010).
15. Gupta, N. & Stopfer, M. Functional analysis of a higher olfactory center, the lateral horn. *J. Neurosci.* **32**, 8138–8148 (2012).
16. Masuda-Nakagawa, L.M., Tanaka, N.K. & O'Kane, C.J. Stereotypic and random patterns of connectivity in the larval mushroom body calyx of *Drosophila*. *Proc. Natl. Acad. Sci. USA* **102**, 19027–19032 (2005).
17. Caron, S.J., Ruta, V., Abbott, L.F. & Axel, R. Random convergence of olfactory inputs in the *Drosophila* mushroom body. *Nature* **497**, 113–117 (2013).
18. Tanaka, N.K., Awasaki, T., Shimada, T. & Ito, K. Integration of chemosensory pathways in the *Drosophila* second-order olfactory centers. *Curr. Biol.* **14**, 449–457 (2004).
19. Gruntman, E. & Turner, G.C. Integration of the olfactory code across dendritic claws of single mushroom body neurons. *Nat. Neurosci.* **16**, 1821–1829 (2013).
20. Murthy, M., Fiete, I. & Laurent, G. Testing odor response stereotypy in the *Drosophila* mushroom body. *Neuron* **59**, 1009–1023 (2008).
21. Pfeiffer, B.D. *et al.* Tools for neuroanatomy and neurogenetics in *Drosophila*. *Proc. Natl. Acad. Sci. USA* **105**, 9715–9720 (2008).
22. de Bruyne, M., Foster, K. & Carlson, J.R. Odor coding in the *Drosophila* antenna. *Neuron* **30**, 537–552 (2001).
23. Hallem, E.A. & Carlson, J.R. Coding of odors by a receptor repertoire. *Cell* **125**, 143–160 (2006).
24. Larsson, M.C. *et al.* Or83b encodes a broadly expressed odorant receptor essential for *Drosophila* olfaction. *Neuron* **43**, 703–714 (2004).
25. Silbering, A.F. *et al.* Complementary function and integrated wiring of the evolutionarily distinct *Drosophila* olfactory subsystems. *J. Neurosci.* **31**, 13357–13375 (2011).
26. Ai, M. *et al.* Acid sensing by the *Drosophila* olfactory system. *Nature* **468**, 691–695 (2010).
27. Liang, L. *et al.* GABAergic projection neurons route selective olfactory inputs to specific higher-order neurons. *Neuron* **79**, 917–931 (2013).
28. Parnas, M., Lin, A.C., Huetteroth, W. & Miesenböck, G. Odor discrimination in *Drosophila*: from neural population codes to behavior. *Neuron* **79**, 932–944 (2013).
29. Couto, A., Alenius, M. & Dickson, B.J. Molecular, anatomical, and functional organization of the *Drosophila* olfactory system. *Curr. Biol.* **15**, 1535–1547 (2005).
30. Jefferis, G.S., Marin, E.C., Stocker, R.F. & Luo, L. Target neuron prespecification in the olfactory map of *Drosophila*. *Nature* **414**, 204–208 (2001).
31. Jefferis, G.S. *et al.* Developmental origin of wiring specificity in the olfactory system of *Drosophila*. *Development* **131**, 117–130 (2004).
32. Yaksi, E. & Wilson, R.I. Electrical coupling between olfactory glomeruli. *Neuron* **67**, 1034–1047 (2010).
33. Lin, H.H., Lai, J.S., Chin, A.L., Chen, Y.C. & Chiang, A.S. A map of olfactory representation in the *Drosophila* mushroom body. *Cell* **128**, 1205–1217 (2007).
34. Kreher, S.A., Mathew, D., Kim, J. & Carlson, J.R. Translation of sensory input into behavioral output via an olfactory system. *Neuron* **59**, 110–124 (2008).
35. Asahina, K., Louis, M., Piccinotti, S. & Vosshall, L.B. A circuit supporting concentration-invariant odor perception in *Drosophila*. *J. Biol.* **8**, 9 (2009).
36. Borst, A. Computation of olfactory signals in *Drosophila melanogaster*. *J. Comp. Physiol. A Neuroethol. Sens. Neural Behav. Physiol.* **152**, 373–383 (1983).
37. Dayan, P. & Abbott, L.F. *Theoretical Neuroscience* (MIT Press, Cambridge, MA, 2001).
38. Rust, N.C., Mante, V., Simoncelli, E.P. & Movshon, J.A. How MT cells analyze the motion of visual patterns. *Nat. Neurosci.* **9**, 1421–1431 (2006).
39. Simoncelli, E.P. Vision and the statistics of the visual environment. *Curr. Opin. Neurobiol.* **13**, 144–149 (2003).

ONLINE METHODS

Fly stocks. Flies were raised in intermediate-density cultures on conventional cornmeal agar medium supplemented with rehydrated potato flakes (Carolina Biological Supply) under a 12 h light, 12 h dark cycle at 25 °C. All experiments were performed on adult female flies within the first 2 days after eclosion. The genotypes used, by figure, are listed in **Supplementary Table 1**. **Supplementary Table 1** also cites previous publications for most of the mutants and transgenic strains in this study, as well as additional detail about unpublished Gal4 lines.

Electrophysiology. *In vivo* whole-cell patch clamp recordings were performed as previously described⁴⁰. Generally, one neuron was recorded per brain. The internal patch pipette solution contained (in mM): 140 potassium aspartate, 10 4-(2-hydroxyethyl)-1-piperazineethanesulfonic acid, 4 MgATP, 0.5 Na₂GTP, 1 ethylene glycol tetraacetic acid, 1 KCl and 13 biocytin hydrazide (pH 7.3, osmolality adjusted to ~268 mOsm). The external saline contained (in mM): 103 NaCl, 3 KCl, 5 N-tris(hydroxymethyl) methyl-2-aminoethane-sulfonic acid, 8 trehalose, 10 glucose, 26 NaHCO₃, 1 NaH₂PO₄, 1.5 CaCl₂ and 4 MgCl₂. The osmolality was adjusted to 270–273 mOsm. The saline was bubbled with 95% O₂ and 5% CO₂ and reached a final pH of 7.3. Recordings were obtained with an Axopatch 200B model amplifier with a CV-203BU head stage and were acquired with custom-written IgorPro or Matlab routines. Recorded voltages and currents were low-pass filtered at 5 kHz before digitization at 10 kHz. Patch pipettes were made from borosilicate glass (Sutter; 1.5-mm outer diameter, 0.86-mm inner diameter) and were fire polished using a microforge (Narishige). For some LHN recordings, the patch pipette was pressure polished to reduce resistance as described previously⁴¹. The estimated final pipette tip opening was submicron in diameter, with the pipette resistance between 10 and 15 MΩ. In randomly targeted PN recordings, PNs were not labeled with a visible marker but were identified on the basis of their cell-body location and characteristic intrinsic properties⁴². In these randomly targeted PN recordings, we made an effort to sample PN somata in both the anterodorsal cluster and the lateral cluster and also to sample both large and small somata, but these recordings are nonetheless probably somewhat biased toward large somata in the anterodorsal cluster. In some paired recordings, we removed one or both antennae to allow for easier access to the antennal lobe. Recordings from DP1m and VA2 PNs were performed using PA-GFP to target our recording electrode to the PN soma (see below). For the paired recording experiments from NP6099 LHNs and DP1m or VA2 PNs, in order to gain the necessary optical and mechanical access to the antennal lobe and lateral horn, we removed the brain from the head capsule and pinned it in a Sylgard-coated dish.

Odor delivery. An air stream (2.005 l per min) was passed through activated carbon and directed at the fly through a carrier tube (6.3-mm inner diameter) and positioned 15 mm from the fly. The fly was positioned to face away from the carrier tube. 5 ml per min of this air stream (the odor stream) was diverted from the carrier and directed by a three-way solenoid valve into the headspace of a clean 1-ml vial (National Scientific, C4011-5W) containing 200 μl of a solution of odor in paraffin oil or an identical empty vial. The solenoid normally directed the odor stream to the empty vial and switched airflow into the odor vial after receiving a command. After passing through either vial, the odor stream joined the carrier stream again. Odor dilutions refer to the dilution factor by volume of odor in solvent. Odor pulses were 500 ms in duration with an interpulse interval of 40 s. Because the odor stream flow rate is relatively low, we reduced the distance the stream had to travel from the solenoid to the vials (9 cm) and from the vials back into the carrier stream (1 cm). Odor dilutions in paraffin oil were prepared fresh daily, and vials were used for only one experiment before they were discarded. Paraffin oil was stripped of low-molecular weight volatiles by storing it under negative pressure, generally for at least several days before use. On the basis of previous work, we know that methyl acetate is relatively selective for DM4 olfactory receptor neurons at low concentrations⁴³, which is relevant to the design of the experiments in **Figure 5**. This previous study used a slightly different olfactometer, but in calibration experiments, we verified that the olfactometer we used in this study delivered, if anything, somewhat more dilute stimuli than those delivered by the previous study at the same nominal dilution.

Two-photon laser scanning microscopy, PA-GFP photoactivation and laser transection. Photoactivation of PA-GFP^{44,45} was performed for anatomical investigation in the lateral horn (**Fig. 1**) and to target PNs for whole-cell recordings in cases for which no specific Gal4 line was available (**Fig. 6**). We used a custom-built two-photon laser scanning microscope running ScanImage acquisition software⁴⁶. For both anatomy and targeting, we used a procedure similar to that described previously^{14,45}. Briefly, the neuropils of interest were identified using the resting fluorescence of PA-GFP at the imaging wavelength (925 nm). After defining volumes of interest on the basis of these background images, PA-GFP was photoconverted by imaging through the volume with 710-nm light. In each photoactivation block, we moved through the z depth of the volume of interest with 0.25-μm steps, imaging each z frame three times. We adjusted the laser power on an experiment-by-experiment basis. After PA-GFP is photoactivated in the neuropil (i.e., axons and dendrites), it diffuses into the somata of the corresponding neurons.

For the anatomical experiments in **Figure 1a**, we photoactivated a large portion of the dorsal lateral horn, taking care not to photoactivate any cell bodies directly. We performed three photoactivation blocks separated by 5-min interblock intervals. On the basis of several experiments similar to that shown in **Figure 1a**, we conservatively estimate that there are at least 12 type I and 24 type II neurons on each side of the brain.

For the physiology experiments in **Figure 6**, we located the desired glomerulus and photoactivated it in a volume of several μm³ that was entirely circumscribed by that glomerulus. In order to confirm that the recorded PN did indeed arborize in the correct glomerulus, we filled every recorded PN with biocytin, visualized it using a fluorescent streptavidin conjugate and inspected it *post hoc* using nc82 antibody to label the glomerular compartments (see below). In these experiments, we performed only one photoactivation block (rather than three) in order to avoid damaging brain tissue before the recording.

For the laser transection experiments shown in **Figure 8a–c**, we labeled the inner antennocerebral tract (iACT) and middle antennocerebral tract (mACT) by expressing GFP under the control of *GH146-Gal4*. The iACT contains the axons of excitatory PNs, and the mACT contains the axons of inhibitory PNs. The iACT was transected between the mushroom body calyx and the lateral horn. The mACT was transected where it appears from beneath the mushroom body peduncle and before it enters the lateral horn. For both transection experiments, we defined volumes of interest that completely circumscribed the tract we aimed to cut. Volumes were approximately 5–10 μm on each side. In order to transect the tract, we scanned through the depth of these volumes once or twice in 0.5-μm steps for approximately 0.5 s of dwell time per frame. The laser power at the back aperture of the objective was 50–80 mW at 800 nm, which is the transection wavelength. The volume, imaging duration and laser power were adjusted on an experiment-by-experiment basis to achieve a visible cavitation bubble that encompassed the axon tract.

Immunohistochemistry and anatomy. In order to ascertain or confirm the glomerular identity of recorded PNs, we filled them with biocytin and visualized the fills with fluorescent-conjugated streptavidin. This was done in two situations. First, every time we recorded from a GFP-labeled PN, we filled it to confirm its putative identity. Second, in random recordings from unlabeled PNs, we filled PNs that turned out to be connected to simultaneously recorded LHNs. To identify glomeruli, the glomerular neuropil was visualized using fluorescence immunohistochemistry with nc82 antibody (Developmental Studies Hybridoma Bank, nc82-s, 1:50 dilution).

In some experiments, the identity of the recorded LHNs was confirmed in a similar manner. The morphology of single dye-filled LHNs was compared with an atlas of brain neuropil divisions (<http://www.virtualflybrain.org/>) in order to determine the region(s) in which LHN axons arborized. Type I neurons arborized in the superior medial protocerebrum, as has been noted previously¹⁸, but their arbors also extended into the superior intermediate protocerebrum and the crepine. Type II neurons arborized in the superior lateral protocerebrum, as has been noted previously¹⁸.

The protocol for processing these fills has been described previously⁴². To reconstruct neuronal morphology from biocytin fills, we hand traced the skeletonized morphology using the Simple Neurite Tracer plugin in Fiji (<http://fiji.sc>)

using the Fill Out command to automatically generate a three-dimensional volume, which we subsequently converted to a z projection. Triple immunofluorescence against GABA (Sigma A2052), CD8 and nc82 (Supplementary Fig. 3) was performed essentially as previously described⁴⁰ except that a different CD8-specific antibody was used (Invitrogen, MCD0800, 1:50) and the nc82 antibody was used at a dilution of 1:50.

Spike detection. Spikes were detected using custom-written Matlab routines. A two-threshold routine was used to detect the events in the voltage trace that were both the fastest to rise and also the fastest to decay (Supplementary Fig. 5). The first threshold was initially used to detect positive peaks in the second time derivative of the voltage trace in order to pick out the fastest-rising events. Next, a threshold was used to detect negative peaks in the first time derivative of the voltage trace in the time window (−0.3 ms, +12 ms) around the second derivative threshold crossing. Both thresholds were set manually and independently for each recording in order to accurately capture the spikes identified by visual inspection. Automated spike detection with this routine was robust at spontaneous and lower odor-evoked firing rates. However, at the higher firing rates produced by type I LHNs, action potential size became very small, and *post hoc* visual inspection became necessary to correct errors. In order to ensure that our results in Figure 5 were not affected by experimenter intervention in spike detection, we blinded the spike detector to the stimulus concentration. In roughly a quarter of the cells we recorded from in our recordings of odor responses, spike sorting could not be performed reliably. Those recordings were excluded from analysis.

Odor response metrics. In cases where we measured odor-evoked spike counts, we counted spikes over a 1-s window starting at the odor-onset command. The odor valve remained open for 500 ms. Because of the construction of our olfactometer, there is a ~150-ms delay from when the odor-onset command is sent by the acquisition computer to the solenoid to the time the odorant reaches the fly, as determined using a fast photoionization detector at the fly's location (mini-PID, Aurora Scientific). As both LHN types showed relatively low levels of spontaneous spiking, we simply counted spikes over a 1-s window starting at the odor-onset command in order to ensure that all odor-evoked spiking was captured. Lifetime sparseness of odor-evoked spike count data was computed as described previously⁴⁷, except that the baseline firing rate (which was always close to zero) was not subtracted from the odor-evoked firing rates.

Spike-triggered averages of postsynaptic voltage. The existence of a monosynaptic connection between a projection neuron and the LHN was assessed using spike-triggered averaging of the LHN membrane potential triggered on single PN spikes. For each trial, we injected a brief (30–100 ms) step of depolarizing current into the PN with the patch pipette to elicit a single action potential. We obtained between 16 and 250 trials for each paired recording. We aligned the postsynaptic voltage trace to the time of the peak of the presynaptic action potential, defined as time $t = 0$. We averaged over the time window $t = -20$ ms to $t = 80$ ms and defined the average voltage in the window -20 ms to 0 ms as the baseline. An excitatory postsynaptic potential (EPSP) was said to occur if in the time window $t = 0$ ms to $t = 5$ ms, the spike-triggered average crossed a threshold of +5 s.d. computed over the 20-ms baseline period. In most experiments, we triggered only single action potentials in PNs, but in four experiments, we also included data from trials in which up to three PN spikes were evoked (using a 100-ms step of current injection in the PN). This could potentially bias EPSP amplitudes; however, these four experiments revealed no connection. EPSP amplitude was measured as the baseline-subtracted peak depolarization in the time window $t = 0$ to $t = 20$ ms. EPSP latency was defined as the time of extrapolated zero crossing of the linear fits to the 20–80% rising phase of the spike-triggered average.

Triplet recordings. In Figure 4b, we measured changes in LHN membrane potential (V_m) while presynaptic PNs were stimulated with a 500-ms step of depolarizing current. For this measurement, V_m was first low-pass filtered to remove spikes. We then computed the average V_m over a steady-state period during the stimulus (100–500 ms after stimulus onset), and we subtracted the average V_m over a baseline period preceding the stimulus.

Modeling. In Figure 4c, we fit LHN spike counts with

$$LHN_{PN1} = R_{max1} \frac{1}{1 + \sigma_1^{n1} / (PN_1)^{n1}}$$

$$LHN_{PN2} = R_{max2} \frac{1}{1 + \sigma_2^{n2} / (PN_2)^{n2}}$$

where PN_1 and PN_2 are the spike counts associated with the first and second PNs, respectively. LHN_{PN1} and LHN_{PN2} are the spike counts of the LHN for trials in which only one PN was active. The equations define input-specific sigmoidal nonlinearities, where the fitted parameters R_{max1} and R_{max2} are the amplitudes of the sigmoids and can be interpreted as the weights associated with the two inputs. The fitted parameter σ is the semisaturation constant (i.e., the level of PN input at which the LHN response is half of the maximum). The fitted exponential parameter n represents the shape and steepness of the sigmoid.

In Figure 4d,e, we fit the three-dimensional transformation from presynaptic spike counts to postsynaptic spike counts with the surface defined by

$$LHN_{total} = LHN_{PN1} + LHN_{PN2}$$

where the parameters were fixed at the values obtained above from fitting the transformation for individual PN inputs. In other words, we predicted the postsynaptic spiking response to the combined activation of two inputs as simply the sum of the responses to each input alone. This model yielded a reasonable prediction of the actual spike counts obtained ($R^2 = 0.69$). Much of the residual variance represents measurement uncertainty (i.e., trial-to-trial or cell-to-cell variation) and so cannot be accounted for by any model of this kind.

We also fit the same data set with an alternative model that incorporates a third term

$$LHN_{total} = LHN_{PN1} + LHN_{PN2} + C(LHN_{PN1} * LHN_{PN2})$$

where the third term represents a multiplicative interaction between the two PN inputs, and C is the coefficient of the interaction term. Again the parameters for LHN_{PN1} and LHN_{PN2} were fixed at the values obtained from fits to individual PN input transformations. This model did not improve fit quality ($R^2 = 0.69$). Furthermore, the fitted coefficient C of the interaction term was two orders of magnitude smaller than R_{max1} and R_{max2} . In other words, there was a minimal contribution from the multiplicative term. This indicates that the data is adequately explained as a sum over PN inputs, and including a cooperative interaction between the two PN inputs provides no additional explanatory power.

Statistics. The appropriate sample size for each experiment was dictated by the magnitude of experiment-to-experiment variation in our pilot data (which was generally low because of the stereotyped properties of these neurons), along with the nature of the hypothesis we sought to test. The decision to use parametric tests of significance throughout this study followed the procedure described by Glantz⁴⁸: inspection of the data indicated that the assumption of normality was reasonable, and so we used parametric tests as a default procedure because these tests are more powerful and more widely used.

40. Wilson, R.I. & Laurent, G. Role of GABAergic inhibition in shaping odor-evoked spatiotemporal patterns in the *Drosophila* antennal lobe. *J. Neurosci.* **25**, 9069–9079 (2005).
41. Goodman, M.B. & Lockery, S.R. Pressure polishing: a method for re-shaping patch pipettes during fire polishing. *J. Neurosci. Methods* **100**, 13–15 (2000).
42. Wilson, R.I., Turner, G.C. & Laurent, G. Transformation of olfactory representations in the *Drosophila* antennal lobe. *Science* **303**, 366–370 (2004).
43. Olsen, S.R., Bhandawat, V. & Wilson, R.I. Divisive normalization in olfactory population codes. *Neuron* **66**, 287–299 (2010).
44. Patterson, G.H. & Lippincott-Schwartz, J. A photoactivatable GFP for selective photolabeling of proteins and cells. *Science* **297**, 1873–1877 (2002).
45. Datta, S.R. *et al.* The *Drosophila* pheromone cVA activates a sexually dimorphic neural circuit. *Nature* **452**, 473–477 (2008).
46. Polgruto, T.A., Sabatini, B.L. & Svoboda, K. ScanImage: flexible software for operating laser scanning microscopes. *Biomed. Eng. Online* **2**, 13 (2003).
47. Perez-Orive, J. *et al.* Oscillations and sparsening of odor representations in the mushroom body. *Science* **297**, 359–365 (2002).
48. Glantz, S.A. *Primer of Biostatistics* (McGraw Hill, New York, 2005).